

Acceleration of tracer and light particles in compressible homogeneous isotropic turbulence

Xiangjun Wang^{1,2}, and Minping Wan^{1,3†} and Luca Biferale⁴

¹Guangdong Provincial Key Laboratory of Turbulence Research and Applications, Department of Mechanics and Aerospace Engineering, Southern University of Science and Technology, Nanshan District, Shenzhen, Guangdong, 518055, China

²Harbin Institute of Technology, Nangang District, Harbin, Heilongjiang, 150090, China

³Southern Marine Science and Engineering Guangdong Laboratory (Guangzhou), 1119 Haibin Road, Nansha District, Guangzhou 511458, China

⁴Department of Physics and INFN University of Rome ‘Tor Vergata’, Via della Ricerca Scientifica 1, 00133 Rome, Italy

(Received xx; revised xx; accepted xx)

The accelerations of tracer and light particles in compressible homogeneous isotropic turbulence (CHIT) is investigated by using data from direct numerical simulations (DNS) up to turbulent Mach number $M_t = 1$. For tracer particles, the flatness factor of acceleration components, F_a , increases gradually for $M_t \in [0.3, 1]$. On the contrary, F_a for light particles develops a maximum around $M_t \sim 0.6$. The PDF of longitudinal acceleration of tracers is increasingly skewed towards the negative value as M_t increases. By contrast, for light particles, the skewness factor of longitudinal acceleration, S_a , firstly becomes more negative with the increase of M_t , and then goes back to 0 when M_t is larger than 0.6. Similarly, differences among tracers and light particles appear also in the zero-crossing time of acceleration correlation. It is argued that all these phenomenons are intimately linked to the flow structures in compression regions, e.g. close to shocklets.

Key words: Authors should not enter keywords on the manuscript, as these must be chosen by the author during the online submission process)

1. Introduction

Much attention has been paid to the investigation of particle-laden turbulence in the past decades. The behaviors of tracer and inertial particles in incompressible turbulence have been studied extensively, as for diffusion, collision and preferential concentration (Jullien *et al.* 1999; Ott & Mann 2000; Boffetta & Sokolov 2002*a,b*; Wang *et al.* 1998; Zhou *et al.* 1998; Yamamoto *et al.* 2001; Sommerfeld 2001; Vance *et al.* 2006; Onishi & Vassilicos 2014; Maxey 1987; Falkovich *et al.* 2002; Wilkinson *et al.* 2006; Chun *et al.* 2005; Goto & Vassilicos 2008; Coleman & Vassilicos 2009; Bragg *et al.* 2015*a,b*). However, there have been much less study of compressible particle-laden turbulence, which are important to understand flow in different domains as, e.g., scramjets (Ferri 1973; Curran *et al.* 1996; Huete *et al.* 2016; Urzay 2018) and the motion of interstellar gas (Barth & Rafkin 2007; Johansen *et al.* 2007; Pan *et al.* 2011). In this

† Email address for correspondence: wanmp@sustech.edu.cn

paper, we will focus mainly on the acceleration statistics of tracer and light particles dispersed in Compressible Homogeneous and Isotropic Turbulence (CHIT), an idealized set-up which could be helpful to the investigation on cavitating flow with clouds of bubbles (Reisman *et al.* 1998; Wang & Brennen 1999; Fuster & Colonius 2011).

Investigation of particle acceleration in turbulence has attracted much attention in the last 20 years. Following the ‘‘K41’’ theory (Kolmogorov 1941*a,b*), the Heisenberg-Yaglom model was proposed to predict the variance of fluid acceleration in homogeneous isotropic turbulence (HIT) (Heisenberg 1985; Yaglom 1949):

$$\langle \mathbf{a}^2 \rangle = a_0 \varepsilon^{3/2} \nu^{-1/2}.$$

Here \mathbf{a} is the acceleration vector, $\langle \cdot \rangle$ represents the ensemble average, a_0 is a universal constant, which was further found to have an anomalous dependency on the Taylor microscale Reynolds number, R_λ , owing to the turbulent intermittency (Yeung & Pope 1989; Voth *et al.* 1998; Vedula & Yeung 1999; Gotoh & Rogallo 1999; Biferale *et al.* 2004). $\varepsilon = 2\nu \langle S_{ij} S_{ij} \rangle$ is the average dissipation rate, S_{ij} is the rate-of-strain tensor, and ν is the kinematic viscosity. Yeung & Pope (1989) numerically found that in HIT for fluid particles, the zero-crossing time (τ_0 , the time in which the autocorrelation function decreases to 0) of acceleration components is around 2.2 times Kolmogorov timescale (τ_η). Moreover, the ratio of τ_0 to τ_η barely varies with Reynolds number, which is supported by later investigations (Yeung 1997; Voth *et al.* 1998; Mordant *et al.* 2004; Biferale & Toschi 2005; Volk *et al.* 2008*a*). Subsequently, Yeung (1997) discovered that τ_0 of the acceleration magnitude is much larger than τ_η . According to the momentum equation, the contribution to fluid acceleration can be decomposed into two parts: pressure gradient term and viscous force term. Vedula & Yeung (1999) pointed out that the contribution of pressure gradient term is dominant over that of viscous force in turbulence. La Porta *et al.* (2001) experimentally confirmed that the acceleration of fluid particles is extremely intermittent in fully developed turbulence. The probability density function (PDF) of acceleration components is well reproduced by a superposition of stretched exponentials (Biferale *et al.* 2004) and the flatness factor of any component, $F_a = \langle (a_i)^4 \rangle / \langle (a_i)^2 \rangle^2$, with $i = 1, 2, 3$, can exceed 60 when R_λ is up to 500. Later on, many investigations on tracer particle acceleration in incompressible flows have been carried out (Voth *et al.* 2002; Mordant *et al.* 2004; Xu *et al.* 2007*b*; Lavezzo *et al.* 2010; Ni *et al.* 2012; Stelzenmuller *et al.* 2017).

Apart from tracer particles, the acceleration of inertial particles (both heavy and light particles) in incompressible turbulent flows also attracted much attention. Bec *et al.* (2006) systematically studied the acceleration statistics of heavy particles in fully developed HIT. They pointed out that the flatness factor and the root-mean square value of particle accelerations both sharply decrease with the increase of the Stokes number, $St = \tau_p / \tau_\eta$, given by the ratio of particle response time and the Kolmogorov flow time. This is a combined effect of preferential concentration on regions with small pressure gradient and filtering due to inertia. Later on, Ayyalasomayajula *et al.* (2006, 2008) proposed a vortex model to describe the selective sampling of turbulent flows and filtering effects. On the contrary, it is known that in HIT light particles enjoys the opposite behaviour, with a strong preferential concentration on high vorticity regions, with a PDF of the acceleration even more intermittent than the tracer case and - in some cases - with longer correlation times when normalized by τ_η (Volk *et al.* 2008*a,b*). Recently, Zhang *et al.* (2019) proposed a theoretical model which successfully predicts the variance of light particles acceleration with different density ratios when St is small (e.g. less than 1.0), as well as the dependence of drag force and inertia force on St .

In recent years, developments of experimental and numerical techniques prompted

a new interest on Lagrangian properties in compressible flows too (Yang *et al.* 2013, 2014, 2016; Zhang *et al.* 2016; Zhang & Xiao 2018; Dai *et al.* 2017, 2018; Xiao *et al.* 2020). Yang *et al.* (2013) investigated the accelerations of tracer particles in CHIT. They found shocklets substantially increase the probability of extremely large-acceleration events. Moreover, almost all the large-acceleration events come from compression regions. Besides, the autocorrelation function of acceleration components near shocklets decreases much faster than that near vortices. Subsequently, Yang *et al.* (2014) studied the influence of shocklets on inertial particles at $M_t \approx 1.0$. They discovered that the PDF of the longitudinal acceleration of light particles in compression regions has a much wider tail at the positive value than that of tracer and heavy particles. It results from the fact that light particles in compression regions have a higher probability to develop a velocity pointing upstream (the low pressure side), compared with tracer and heavy particles. Recently, Haugen *et al.* (2021) studied the clustering of heavy particles in two different compressible isotropic flows: compressively forced turbulence and solenoidally forced turbulence. They found that the clustering of particles in compressively forced turbulence peaks at two different St. The first peak (at lower St) results from the contribution of shocklets and the other is attributed to the centrifugal sling effect.

In this paper, we present a systematic investigation of light particles accelerations statistics at high Reynolds numbers and at changing the degree of compressibility, i.e. the turbulent Mach number and the results will be compared with those of tracer particles. In particular, we are interested to characterize the role played by the presence of shocklets at changing M_t concerning both the single time PDF of bubbles acceleration and its temporal correlation. One of the main result, is the identification of a *critical* Mach number, $M_t \sim 0.6$ where the statistics of light particles strongly departs from the one of tracers. The outline of the paper is as follow: the numerical details are introduced in Section 2. The more important results and analysis are described in Section 3. Finally, a brief conclusion and discussion will be given in Section 4.

2. Simulation configuration

The three-dimensional CHIT was simulated in a periodic cubic box with each side length of 2π , based on a hybrid scheme (Wang *et al.* 2010) which combines the seventh-order weighted essentially non-oscillatory (WENO) scheme and eighth-order compact central finite difference scheme. The dimensionless governing equations of compressible turbulent flow are shown below:

$$\frac{\partial \rho_f}{\partial t} + \nabla \cdot (\rho_f \mathbf{u}) = 0 \quad (2.1)$$

$$\frac{\partial \rho_f \mathbf{u}}{\partial t} + \nabla \cdot (\rho_f \mathbf{u} \mathbf{u}) = -\nabla \left(\frac{p}{\gamma M^2} \right) + \frac{1}{\text{Re}} \nabla \cdot \boldsymbol{\sigma} + \mathbf{f} \quad (2.2)$$

$$\frac{\partial \mathcal{E}}{\partial t} + \nabla \cdot \left[\left(\mathcal{E} + \frac{p}{\gamma M^2} \right) \mathbf{u} \right] = \frac{1}{\alpha} \nabla \cdot (\kappa \nabla T) + \frac{1}{\text{Re}} \nabla \cdot (\boldsymbol{\sigma} \cdot \mathbf{u}) + \mathbf{f} \cdot \mathbf{u} + \Lambda \quad (2.3)$$

$$p = \rho_f T \quad (2.4)$$

where ρ_f , \mathbf{u} and p separately represent the density, velocity and static pressure of fluid. γ is the ratio of the specific heat at constant pressure, C_p , to the specific heat at constant volume, C_v . $\boldsymbol{\sigma} = \mu [\nabla \mathbf{u} + (\nabla \mathbf{u})^T] - \frac{2}{3} \mu \theta \mathbf{I}$ is the viscous stress, where μ is the dynamic viscosity, $\theta = \nabla \cdot \mathbf{u}$ is the divergence of fluid velocity and \mathbf{I} is the identity matrix. Also, $M = U_0/c_0$ and $\text{Re} = \rho_0 U_0 L_0 / \mu_0$ are the reference Mach number and Reynolds

R_λ	M_t	N^3	ν	ε	η	τ_η	u_{rms}	L_f	T_f
123	0.36	512^3	4.17E-3	0.73	1.78E-2	7.59E-2	2.28	1.47	1.12
122	0.51	512^3	4.18E-3	0.78	1.75E-2	7.36E-2	2.30	1.45	1.09
122	0.64	512^3	4.20E-3	0.74	1.78E-2	7.55E-2	2.29	1.46	1.10
122	0.77	512^3	4.23E-3	0.69	1.82E-2	7.84E-2	2.27	1.48	1.13
119	0.89	512^3	4.27E-3	0.70	1.83E-2	7.84E-2	2.27	1.48	1.13
117	1.00	512^3	4.31E-3	0.63	1.89E-2	8.28E-2	2.23	1.51	1.17

TABLE 1. Simulation parameters: Taylor Reynolds number R_λ , turbulent Mach number M_t , grid points N^3 , kinematic viscosity ν , average dissipation rate of kinetic turbulent energy ε , Kolmogorov length scale η , Kolmogorov time scale τ_η , root-mean-square fluctuation velocity $u_{rms} = \sqrt{\langle u_i u_i \rangle}$, integral length scale $L_f = 3\pi/(2u_{rms}^2) \int_0^{+\infty} [E(k)/k] dk$ and large-scale eddy turnover time $T_f = \sqrt{3}L_f/u_{rms}$.

number. Here, L_0 , ρ_0 , U_0 , μ_0 and c_0 are the reference length, density, velocity, dynamic viscosity and speed of sound separately. $\mathcal{E} = p/[(\gamma - 1)\gamma M^2] + \frac{1}{2}\rho_f \mathbf{u} \cdot \mathbf{u}$ is the total energy per unit volume. T denotes the temperature and κ is the thermal conductivity. $\alpha = \text{PrRe}(\gamma - 1)M^2$ is a coefficient from nondimensionalization, and Pr is the reference Prandtl number, which is specified as 0.7 in this paper. To maintain a stationary flow, an external force (\mathbf{f}) is applied on the solenoidal velocity components at large scales (the first two wavenumbers). Besides, a uniform cooling term (Λ) is used to keep the internal energy steady. The detailed description about the forcing and cooling mechanism was introduced in Wang *et al.* (2010), Federrath *et al.* (2010) and Kida & Orszag (1990). In this paper, the turbulent Mach number (M_t) varies from 0.36 to 1.00 with Taylor Reynolds number $R_\lambda \approx 120$ and the total grid number (N^3) in the computational domain is 512^3 . Detailed parameters of the simulations are listed in Table 1.

The light particles are regarded as point objects, neglecting the influence of particles on turbulent flows and their mutual interaction. The motion of light particles is governed by:

$$\frac{d\mathbf{x}_p}{dt} = \mathbf{v}_p \quad (2.5)$$

$$\frac{d\mathbf{v}_p}{dt} = \frac{\mathbf{u}_p - \mathbf{v}_p}{\tau_p} + \beta \frac{D\mathbf{u}_p}{Dt} \quad (2.6)$$

$$\tau_p = \frac{\rho_f d^2}{12\beta\mu} \quad (2.7)$$

$$\beta = \frac{3\rho_f}{2\rho_p + \rho_f} \quad (2.8)$$

where \mathbf{x}_p , \mathbf{v}_p , τ_p and d are the position, velocity, response time and diameter of particles, respectively, and \mathbf{u}_p is the velocity of the flow at the position of the particle. μ is the dynamic viscosity of fluid at the position of particles, and we notice that both τ and β are dependent on space and time due to the variation of the underlying fluid velocity ρ_f . As a result, in a compressible flow, even particle with a density ρ_p equal to the average flow density $\langle \rho_f \rangle$ will nevertheless be locally subjected to inertial forces due to the variation of the local flow density. In our case we have chosen $\rho_p = 0.01\langle \rho_f \rangle$ for the light particles. It is important to stress that Eq. (2.6) must be considered an approximation of the true point-like description of inertial forces. Beside corrections present also in incompressible forces, as the Faxen and Basset terms (Maxey & Riley 1983; Gatignol 1983), here we

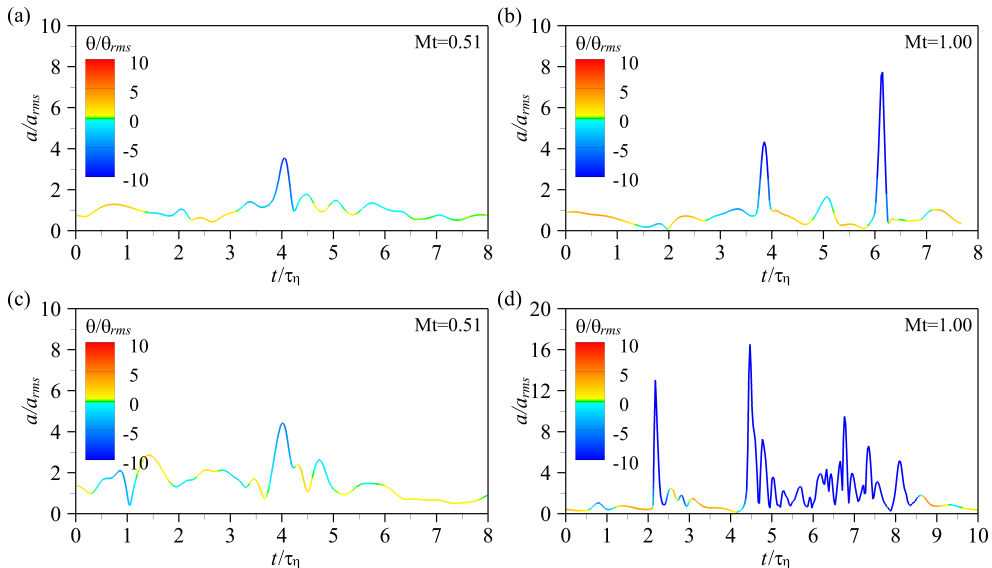


FIGURE 1. The evolution of the acceleration magnitude, a , of typical tracers (a-b) and light particles (c-d) at $M_t = 0.51$ and $M_t = 1.00$. The colorbar indicates the divergence of fluid velocity, θ , at the position of particles. Here a_{rms} and θ_{rms} separately represent the root mean square value of a and θ .

need to consider also new forces induced by density variations of the fluid flow at the particle positions (Parmar *et al.* 2011, 2012). In appendix A we present a thoughtful discussion about these new effects and show that at moderate Mach numbers, as the one here investigated, they can be most of the time safely neglected. The fluid velocity at the position of particles, \mathbf{u}_p , is evaluated by a fourth-order Lagrangian interpolation. The operator, D/Dt , represents the material derivative. 256^3 particles are uniformly released into the computational domain after the flow reaches a statistically steady state. After the particles are fully mixed, we sample over 15 times large eddy turnover time (T_f) to explore the spatial, instantaneous statistics of particles. The Stokes number ($St = \tau_p/\tau_\eta$) of particles is approximately 0.21, and the average of β is around 2.94. In addition, tracer particles whose velocity follows the local fluid velocity are also analyzed for comparison.

3. Results and analysis

Before presenting the results from the statistical analysis, we show in Figure 1 some characteristic evolution of the acceleration magnitudes, a , along tracers and light particles trajectories near strong compression structures (e.g. shocklets) at $M_t = 0.51$ and $M_t = 1.00$, color coded in terms of the local fluid compressibility θ . For tracer particles, there is no significant difference between $M_t = 0.51$ and 1.00, except for the larger peak of acceleration magnitudes near shocklets at $M_t = 1.00$. For light particles at $M_t = 0.51$, the evolution of acceleration magnitudes is similar to that of tracer particles. However, at $M_t = 1.00$, light particles seem to be trapped near the shocklets for a long time (several times τ_η), and the acceleration magnitudes of particles fluctuate dramatically.

The probability density functions (PDFs) of one component of the particle accelerations, a_i , with $i = 1, 2, 3$, are illustrated in Fig. 2. It is apparent that all PDFs have some intense stretched tails, indicating that the accelerations of tracer and light particles are both intermittent. The strength of intermittency can be quantified by the

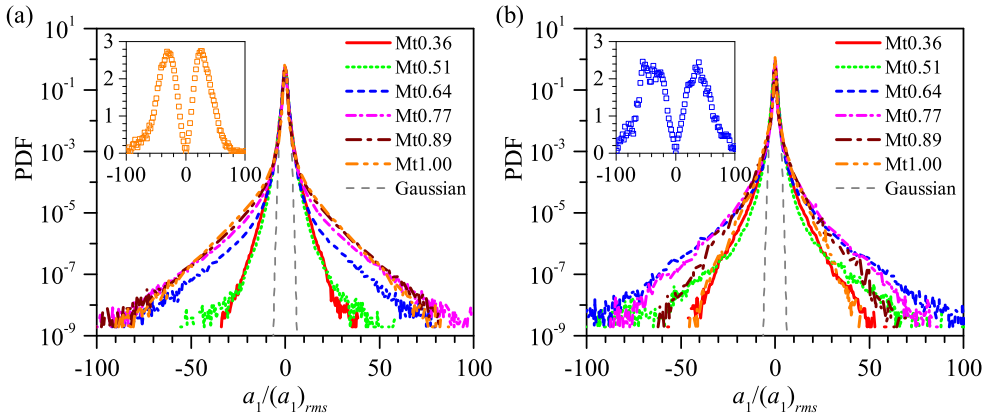


FIGURE 2. The probability density functions (PDFs), $P(a_i)$, of one component of the accelerations a_i , normalized with its root mean square. Because of isotropy all three components are equivalent. For clarity here we show only the case with $i = 1$. (a) is for tracer particles. Inset: $(a_1)^4 P(a_1)$, at $M_t = 1.00$, is presented to check the statistical convergence of the fourth-order moments; (b) is for light particles. Inset: $(a_1)^4 P(a_1)$ is shown at $M_t = 0.64$.

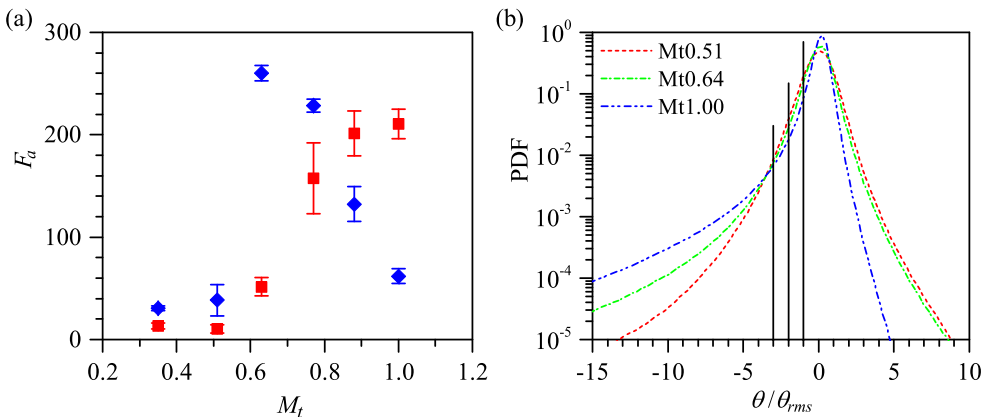


FIGURE 3. Panel (a): the flatness factor of particle acceleration components, F_a , at changing M_t for tracers (red squares) and light particles (blue diamonds). The error bar is calculated from the scatter among 30 subsamples obtained from 30 time snapshots. Panel (b): the PDFs of compressibility θ in the whole computational domain at $M_t = 0.51, 0.64$ and 1.00 . The three vertical lines mark the values CR1, CR2 and CR3 where $\theta < -\theta_{rms}$, $\theta < -2\theta_{rms}$ and $\theta < -3\theta_{rms}$.

flatness (or kurtosis). For tracer particles, the flatness of acceleration components, F_a , steadily increases with the increase of M_t , as seen in Fig. 3 (a). Here, F_a is defined as: $F_a = \langle (a_1)^4 \rangle / \langle (a_1)^2 \rangle^2$. The operator $\langle \cdot \rangle$ means the average among particles. However, F_a of light particles does not follow this trend. As M_t increases from 0.36 to 1.00, F_a of light particles firstly increases, then followed by a reduction after M_t exceeds about 0.6. In order to explain this phenomenon, we define the compression regions: CR1, CR2 and CR3 representing the regions with $\theta < -\theta_{rms}$, $\theta < -2\theta_{rms}$ and $\theta < -3\theta_{rms}$ separately, as shown in Fig. 3 (b). Then, it is found that the stretched tails of acceleration PDFs predominantly result from the particles in strong compression regions when M_t is large, as shown in Fig. 4. The increase of F_a of tracer particles (also applicable for light particles at $M_t < 0.6$), is attributed to the fact that increasing compressibility increases the flow

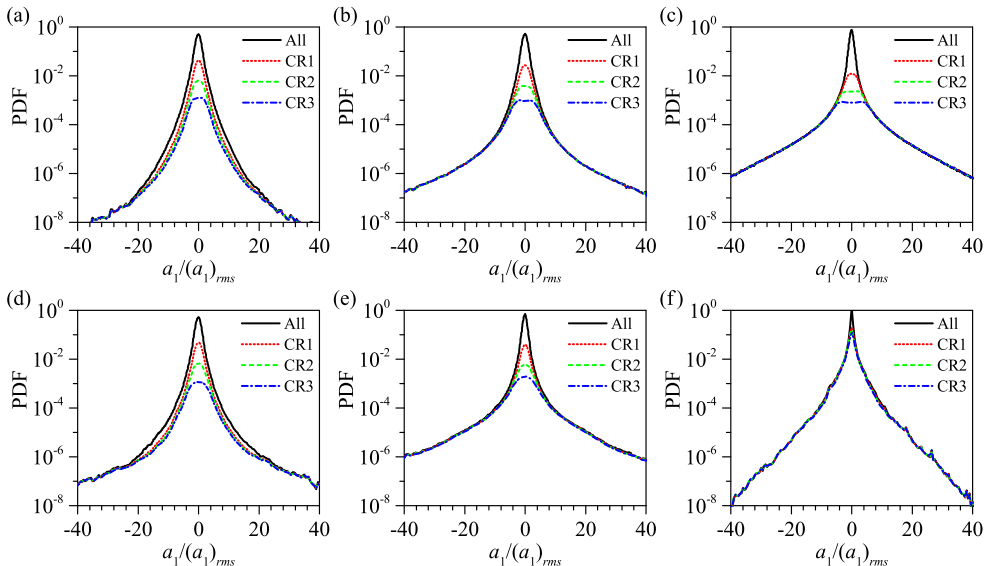


FIGURE 4. The probability density functions (PDFs) of particle acceleration components. (a)-(c) is for tracer particles at $M_t=0.51$, 0.64 and 1.00 respectively; (d)-(f) is for light particles at $M_t=0.51$, 0.64 and 1.00 . The black solid line is the PDF of a_1 for particles in the whole computational domain; the red dotted line, green dashed line and blue dash-dotted line represent the contribution of particles in CR1, CR2 and CR3 separately.

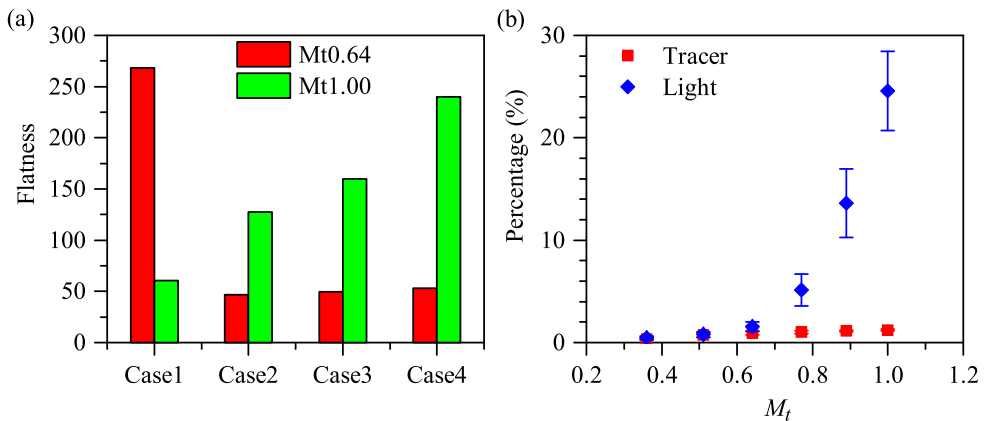


FIGURE 5. Panel (a): F_a of light particles in different regions. Here, Case 1: the whole domain; Case 2: the regions with $\theta > -3\theta_{rms}$; Case 3: the regions with $\theta > -2\theta_{rms}$; Case 4: the regions with $\theta > -\theta_{rms}$. Panel (b): the ratio of the particle number in CR3 to the total particle number in the whole domain.

intermittency too. However, when M_t is larger than 0.6, why does F_a of light particles decrease with the increase of M_t ? In the following we argue that it is related to certain phenomena of light particles in compression regions.

Let us first compare the F_a of light particles in different regions, as shown in Fig. 5 (a), where Case 1 represents the whole domain; Case 2 represents the region with $\theta > -3\theta_{rms}$ (removing CR3 from Case 1); Case 3 represents the region with $\theta > -2\theta_{rms}$ (removing CR2 from Case 1); Case 4 represents the region with $\theta > -\theta_{rms}$ (removing CR1 from Case 1). We can notice that at $M_t = 0.64$, F_a decreases sharply once the light particles in

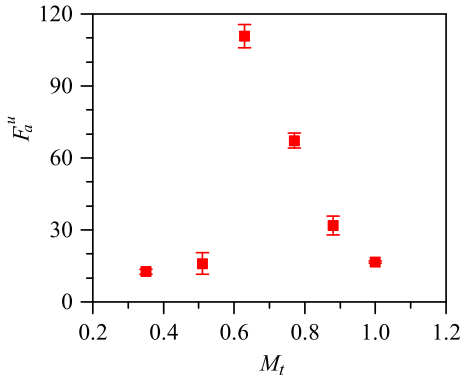


FIGURE 6. The flatness factor of acceleration components of fluid elements at the position of light particles, F_a^u , versus M_t .

CR3 are removed. In contrast, at $M_t = 1.00$, F_a increases steadily as the particles in CR3, CR2 and CR1 are removed. To explain this difference, we further measure the number of light particles in CR3, see Fig. 5 (b), where the number of tracer particles in CR3 slightly increases as M_t increases from 0.36 to 1.00. However, the number of light particles in CR3 dramatically increases when $M_t > 0.6$. Especially at $M_t = 1.00$, it accounts for approximate 25% of the total particle number in the whole domain. According to Fig. 4, ones can understand that the extremely large accelerations of particles mainly come from the strong compression regions (such as CR3). Then, if the number of particles in CR3 is small (like tracers), the probability of the large accelerations is still small. Therefore, a slight increase of particle number in CR3 will make a contribution to the enhancement of the acceleration intermittency. Hence, F_a of tracer particles increases with the increase of M_t . On the other hand, if the number of particles in CR3 is too large (like light particles at $M_t = 0.77 - 1.00$), there will be a large portion of particles with large accelerations. Namely, most of them cannot be regarded as rare events any more. Then, the increase of particle number in CR3 will not contribute to the increase of acceleration intermittency any more. Mathematically, large amount of particles accumulating in CR3 will cause a significant increase of the standard deviation of accelerations (σ_a). And the increase of $(\sigma_a)^4$ is faster than the increase of the forth-order moment of accelerations. In conclusion, the preferential concentration of light particles in strong compression regions (e.g. CR3) results in the decrease of F_a when $M_t > 0.6$. In order to further validate this mechanism, the flatness factor of acceleration components of fluid elements at the position of light particles, F_a^u , is measured, shown in Fig. 6 where F_a^u varies with the same trend as F_a of light particles.

3.1. Longitudinal acceleration at different M_t

Figure 7 presents the PDFs of particle longitudinal accelerations (\mathbf{a}_L) at $M_t = 0.36 - 1.00$. Ones can see that for tracer particles, the PDFs of \mathbf{a}_L all skew to the negative value. However, for light particles, the PDFs of \mathbf{a}_L only moderately skew to the negative value at low M_t (e.g. $M_t = 0.51$), and this trend vanishes as the PDFs become almost symmetric at high M_t (e.g. $M_t = 1.00$). To quantify this difference, we measure the skewness factor of \mathbf{a}_L , S_a , as shown in Fig. 8. For tracer particles, S_a becomes more negative as M_t increases from 0.36 to 1.0. As well known, shocklets will appear in compression regions with the increase of M_t . When tracer particles pass through the shocklets from upstream to downstream, they will be decelerated significantly owing to

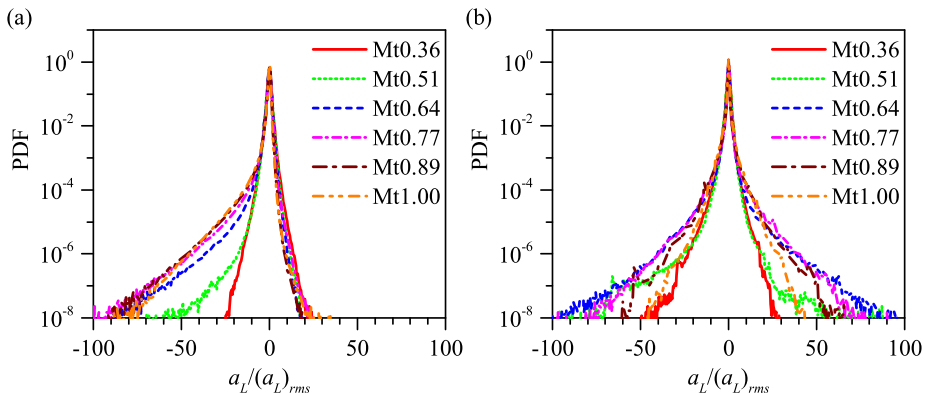


FIGURE 7. The PDFs of longitudinal accelerations. (a) is for tracer particles; (b) is for light particles.

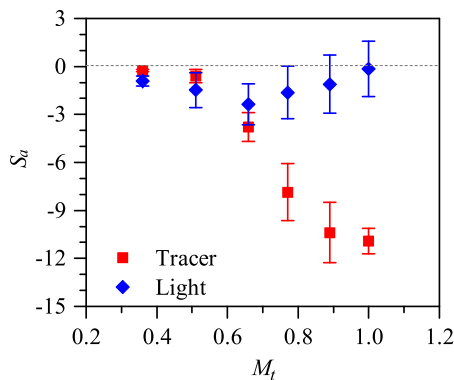


FIGURE 8. The skewness factor of particle longitudinal accelerations, S_a , varies with M_t .

the negative pressure gradient (Anderson Jr 2010). As M_t increases, the shocklets become stronger (the deceleration is also more remarkable). Therefore, the PDF of \mathbf{a}_L is more skewed to negative value and S_a becomes more negative for tracer particles when M_t increases.

As shown in Fig. 8, for light particles, S_a also decreases with M_t when M_t is small, similar to that of tracer particles. However S_a gradually goes back to zero after $M_t > 0.6$. A similar phenomenon was suggested by Yang *et al.* (2014), who discovered that S_a of light particles in compression regions is close to 0 at $M_t \approx 1.03$, and there are many light particles whose velocities have an obtuse angle with local pressure gradient. To understand the above difference between tracers and light particles, we show in Fig. 9 the PDF of the angle between particle velocity and pressure gradient, α , in CR1 (compression region with $\theta < -\theta_{rms}$). One can see that most tracer particles in CR1 have an angle of $\alpha < 90^\circ$ at all M_t . However, for light particles, the number of particle with $\alpha > 90^\circ$ steadily increases as M_t increases from 0.6 to 1.0. We then track the particles in CR1 and statistically measure how many of them have an angle of $\alpha < 90^\circ$ when they enter CR1, denoted as N_{CR1}^{in} . Also, the number of particles with $\alpha < 90^\circ$ in CR1 at one time point is statistically measured, defined as N_{CR1} . Figure 10 shows that for tracer particles, N_{CR1} is always close to N_{CR1}^{in} at different M_t . Namely, tracer particles rarely change their direction of movement in CR1. However, for light particles, N_{CR1} is noticeably smaller

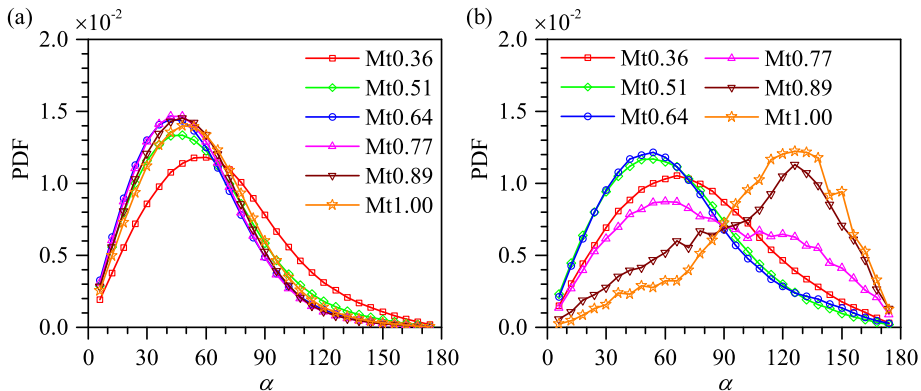


FIGURE 9. The PDFs of angle (α) between the velocity of particles and the pressure gradient at the position of particles in compression regions. (a) is for tracer particles; (b) is for light particles.

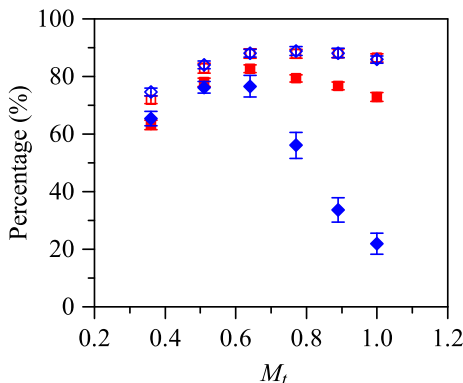


FIGURE 10. The ratio of N_{CR1}^{in} (red squares) and N_{CR1} (blue diamonds) to the total number of particles in CR1. The empty symbols are for tracer particles and the filled symbols are for light particles.

than N_{CR1}^{in} at high M_t , and this deviation becomes more significant as M_t increases. That is, as M_t increases, more light particles reverse their direction of velocity from $\alpha < 90^\circ$ to $\alpha > 90^\circ$ in CR1, so that more light particles which were decelerated turn to be accelerated. This is the main reason for the PDF of \mathbf{a}_L being more symmetric when $M_t > 0.6$. Besides, N_{CR1} of light particles decreases moderately as M_t increases from 0.6 to 1.0, which implies that at high M_t , more light particles have positive longitudinal accelerations when they are entering CR1. It is also a factor that S_a of light particles goes back to 0.

Why do many light particles reverse their velocity direction from $\alpha < 90^\circ$ to $\alpha > 90^\circ$ in CR1, but few tracer particles do? It can be seen in Eq. (2.6) that the effect of local fluid acceleration (the second term on the right-hand side) on light particles was amplified by β (for light particles, $\beta \approx 2.94$ in our simulations). Thus, light particles are easier to be decelerated by the negative pressure gradient near shocklets as the dominant contribution to fluid acceleration comes from pressure gradient. After light particles enter compression regions from upstream, their direction of velocity is more likely to be reversed near shocklets, and this trend will be more remarkable as M_t increases.

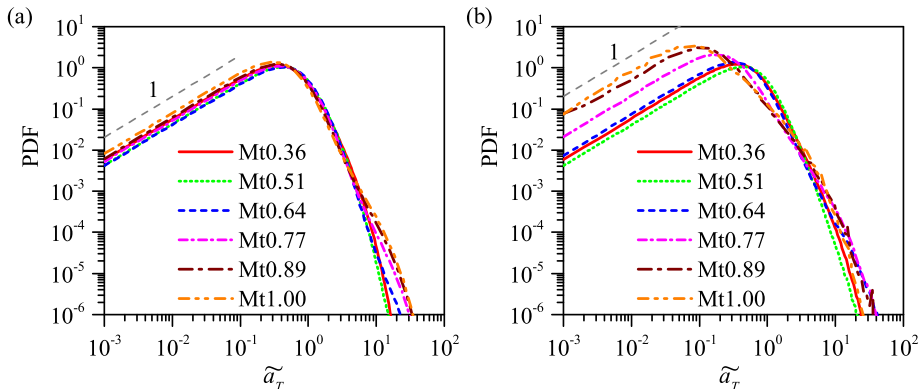


FIGURE 11. The PDFs of \tilde{a}_T at different M_t . (a) is for tracer particles; (b) is for light particles.

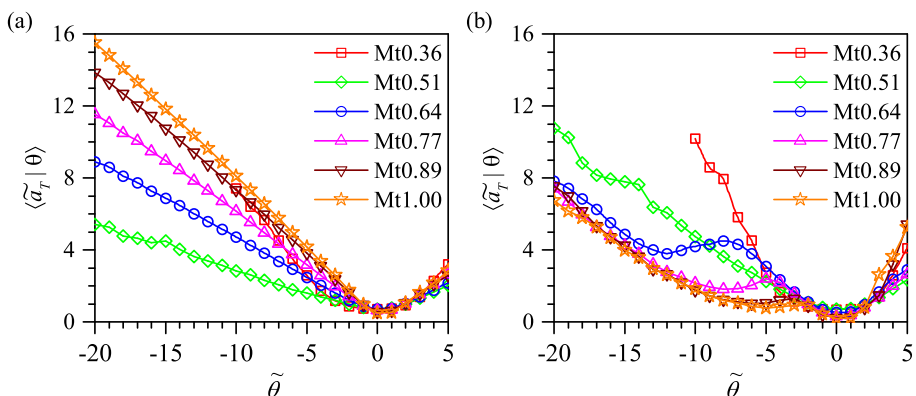


FIGURE 12. $\langle \tilde{a}_T | \theta \rangle$ varies with $\tilde{\theta}$ at different M_t . (a) is for tracer particles; (b) is for light particles.

3.2. Transverse acceleration at different M_t

The change of velocity direction is intimately linked to the transverse acceleration (\mathbf{a}_T). In Figure 11 (a) we show the PDFs of normalized transverse acceleration magnitudes, $\tilde{a}_T = a_T / (a_T)_{rms}$, of tracer particles at different M_t , where a_T is the magnitude of transverse acceleration. When \tilde{a}_T is not large (e.g. $\tilde{a}_T < 3$), the PDFs of \tilde{a}_T are close to each other for the cases with different M_t . However, when $\tilde{a}_T > 3$, the PDFs display slightly wider tails at higher M_t . This implies that when \tilde{a}_T is small, it is mainly influenced by vortices, rather than shocklets. The exist of shocklets only increases the probability of large \tilde{a}_T . On the contrast, the PDFs of \tilde{a}_T of light particles are quite distinguishing at different M_t , as illustrated in Fig. 11 (b) where at higher M_t , the probability of small \tilde{a}_T is larger, indicating that \tilde{a}_T of light particles is easier to be influenced by shocklets than that of tracer particles. In addition, when \tilde{a}_T is quite small, the PDFs all linearly scale with \tilde{a}_T , which can be explained by the model developed by Xu *et al.* (2007a). The three acceleration components of particles can be regarded as independent Gaussian random variables when their magnitude is quite close to zero. Then, a_T of particles will follow a χ distribution with 2 degrees of freedom, leading to a linear dependency for small enough \tilde{a}_T .

Furthermore, we have measured the average of \tilde{a}_T conditioned for a given velocity divergence, $\langle \tilde{a}_T | \theta \rangle$, shown in Fig. 12. For tracer particles, except for $M_t = 0.36$, $\langle \tilde{a}_T | \theta \rangle$

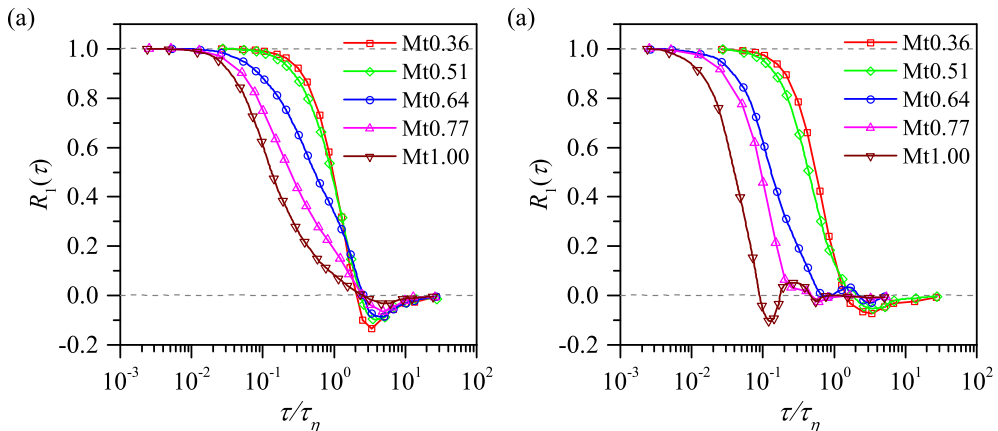


FIGURE 13. The autocorrelation function, $R_1(\tau)$, of a_1 at different M_t . (a) is for tracers; (b) is for light particles.

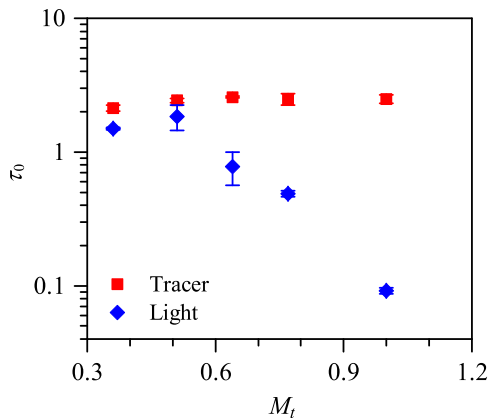


FIGURE 14. τ_0 varies with M_t for tracers (red squares) and light particles (blue diamonds).

linearly increases with the decrease of $\tilde{\theta}$ ($\tilde{\theta} = \theta/\theta_{rms}$) in compression regions, and it gradually increases with the increase of M_t , for a given $\tilde{\theta}$. On the other hand, for light particles, the linear increase of $\langle \tilde{a}_T|\theta \rangle$ with the decrease of $\tilde{\theta}$ does not appear in compression regions. Particularly when $M_t > 0.6$, there is always a section where $\langle \tilde{a}_T|\theta \rangle$ decreases as $\tilde{\theta}$ decreases.

3.3. Autocorrelation function of acceleration components at different M_t

Figure 13 shows the autocorrelation function of first component of the acceleration $R_1(\tau) = \langle a_1(t)a_1(t+\tau) \rangle / \langle a_1(t)^2 \rangle$ (because of isotropy R_2 and R_3 would be equal to R_1). One can notice that for tracer particles, the zero-crossing time (τ_0) barely varies with M_t and it is approximately close to $2.3\tau_\eta$, which is similar to the results in incompressible turbulence (Yeung 1997; Mordant *et al.* 2004; Volk *et al.* 2008a). Here, τ_0 denotes the time in which $\rho_1(\tau)$ decreases to 0. For light particles, τ_0 is also approximate to $2.3\tau_\eta$ when $M_t < 0.6$. However, as M_t increases further, τ_0 gradually decreases, as shown in Fig. 14.

Why is the behavior of τ_0 between tracer and light particles different from each other? Yang *et al.* (2013) found that the autocorrelation function of acceleration of

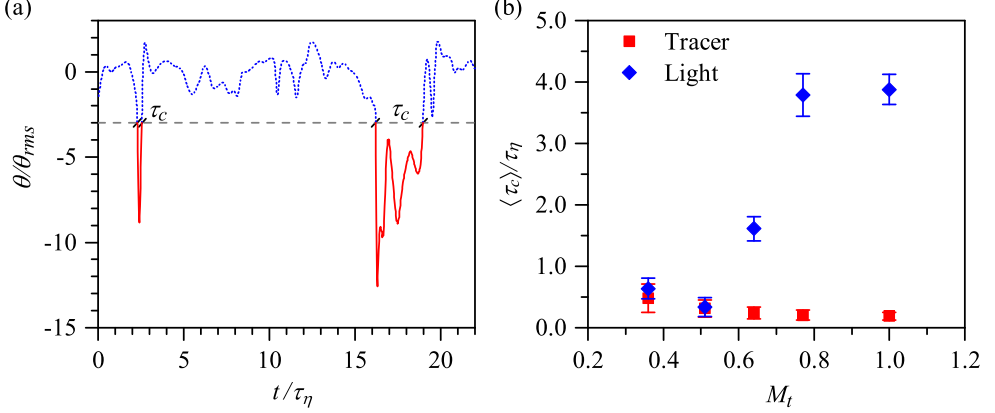


FIGURE 15. Panel (a): the history curve of θ along one trajectory of light particles at $M_t = 1.00$. Here τ_c denotes the time over which particles pass through CR3. Panel (b): the average value of characteristic time of particles staying in CR3, $\langle \tau_c \rangle$, at different M_t .

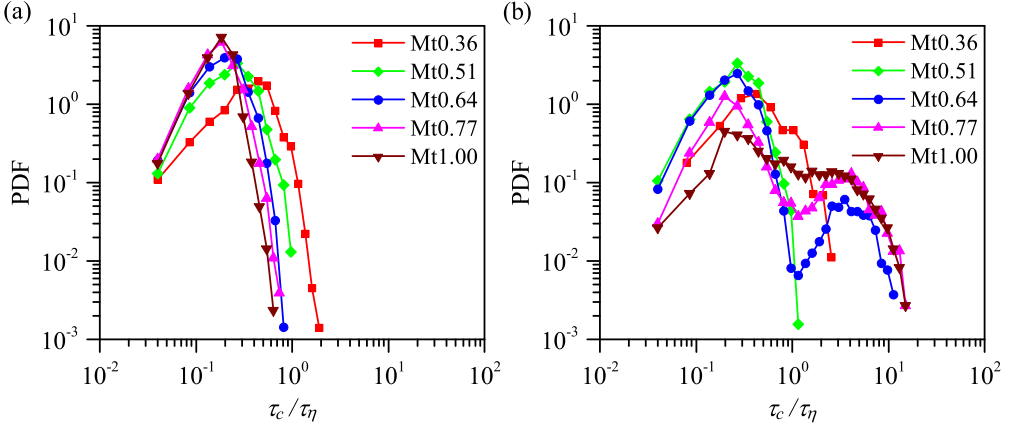


FIGURE 16. The PDF of the time (τ_c) that particles stay in strong compression regions (CR3) at different M_t . (a) is for tracers; (b) is for light particles

tracer particles near shocklets decreases much faster than that near vortices in CHIT. In addition, we use τ_c to denote the time over which particles pass through the strong compression regions (CR3), as shown in Fig. 15 (a). It is found that the average of τ_c among tracer particles, $\langle \tau_c \rangle$, is distinctly smaller than τ_η and it slightly decreases with the increase of M_t ($\langle \tau_c \rangle \approx 0.2\tau_\eta$ at $M_t = 1.00$), as shown in Fig. 15 (b). For light particles, $\langle \tau_c \rangle$ is similar to that of tracer particles when $M_t < 0.6$. However, as M_t further increases, $\langle \tau_c \rangle$ increases dramatically, up to around $4\tau_\eta$ at high M_t . Then, it can be speculated that $R_1(\tau)$ is barely influenced by shocklets since the time that tracer particles stay in strong compression regions (near shocklets) is quite short, so that $\rho_1(\tau)$ should be mainly influenced by vortices. Therefore, $\tau_0 \approx 2.34\tau_\eta$ of tracer particles is independent of M_t and close to the small eddy turnover time. For light particles, at low M_t (e.g. $M_t = 0.51$), $\langle \tau_c \rangle$ is similar to that of tracers so that τ_0 of light particles is quite close to that of tracer particles. However, as M_t increases, $\langle \tau_c \rangle$ of light particles increases gradually because more light particles will be trapped in strong compression regions (near shocklets) for several τ_η , as shown in Fig. 16 (b) where the PDFs of τ_c of light particles present two peaks when $M_t > 0.6$, at difference from what happens for tracers (seen in

Fig. 16 (a)). The position of first peak ($\tau_c/\tau_\eta = 0.2 - 0.3$) is similar to that of tracer particles. However, the second peak occurs in the range of $\tau_c/\tau_\eta = 3.0 - 4.0$, indicating that many light particles are trapped by shocklets, hence, the influence on $R_1(\tau)$ becomes remarkable. Therefore, τ_0 will be influenced by both shocklets and vortices at high M_t , and as M_t increases, τ_0 of light particles decreases, as shown in Fig. 13(b), since more light particles are trapped near shocklets.

4. Conclusion and Discussion

The acceleration statistics of tracer and light particles in CHIT have been studied. Our main finding is related to the characteristic signature of the presence of shocklets in the probability distribution function of acceleration and on its characteristic correlation times. In particular, we found that at $M_t \sim 0.6$ the statistical properties of light particles acceleration start to be strongly different from the one of the underlying tracers, developing a sort of *condensation* on and near shocklets structures, where a high percentage of the total number of particles is concentrated. As a consequence, acceleration flatness, skewness and autocorrelation time are strongly affected. We find that in the range here investigated $M_t \in [0.31, 1]$ the flatness factor of acceleration components, F_a , of tracers increases monotonically with M_t . For light particles, F_a also increases with M_t at $M_t < 0.6$. However, when $M_t > 0.6$, F_a of light particle decreases with M_t because of preferential accumulation in strong compression regions.

The PDFs of the longitudinal acceleration of tracer particles are found to be skewed towards negative value, and as M_t increases, the skewness factor, S_a , becomes more negative. For light particles, S_a also becomes more negative with the increase of M_t , then followed by a tendency to return to 0 after $M_t > 0.6$. We attribute the tendency of the longitudinal acceleration PDF of light particles to become more and more symmetric at high M_t to the fact that more particles reverse their direction of velocity from $\alpha < 90^\circ$ to $\alpha > 90^\circ$ in compression regions (e.g. the regions with $\theta < -\theta_{rms}$) at increasing compressibility. Together with the fact that more light particles with positive longitudinal acceleration enter compression regions at higher M_t .

For tracers, when the normalized transverse acceleration magnitude, \tilde{a}_T , is not large (e.g. $\tilde{a}_T < 3$), the PDFs of \tilde{a}_T are close to each other for different M_t . This implies that when \tilde{a}_T is small, \tilde{a}_T is mainly influenced by vortices, rather than shocklets. On the contrast, for light particles, the PDFs of \tilde{a}_T are quite distinguishing for different M_t . At higher M_t , the probability of small \tilde{a}_T is much larger, indicating that \tilde{a}_T of light particles is easier to be influenced by shocklets than that of tracer particles.

We have found that for tracer particles, the characteristic time, τ_c , near shocklets is quite short, especially at high M_t ($\langle \tau_c \rangle \approx 0.2\tau_\eta$ at $M_t = 1.00$). Then, the autocorrelation function of accelerations is barely influenced by shocklets. As a result, the zero-crossing time, τ_0 , does not vary too much with M_t . For light particles, as M_t increases, more particles are trapped near shocklets for several τ_η so that the influence of shocklets on the autocorrelation function of accelerations becomes remarkable. Therefore, τ_0 is greatly influenced by shocklets and decreases with M_t .

The strong singular signature of shocklets for the dynamic and statistics of light particles opens many important questions that needs further numerical and experimental studies. In particular, the role of correction terms to the Eq. (2.6) induced by the presence of compressibility must be better elucidated as discussed in Appendix A. Second, in the presence of strong particles' concentration nearby shocklets, the importance of bubble-bubble collision, breakup and coalescence should be better quantified, as well as their feedback on the flow.

We are grateful to Prof. Jianchun Wang for providing us the DNS code for CHIT. This work is funded by the National Numerical Wind Tunnel Project (No. NNW2019ZT1-A01), the National Natural Science Foundation of China (Grant No. 91752201), the Department of Science and Technology of Guangdong Province (Grant No. 2019B21203001), Key Special Project for Introduced Talents Team of Southern Marine Science and Engineering Guangdong Laboratory (Guangzhou) (Grant No. GML2019ZD0103), and by the Shenzhen Science and Technology Innovation Committee (Grant No. KQTD20180411143441009). We acknowledge computing support provided by the Center for Computational Science and Engineering of the Southern University of Science and Technology. L.B. acknowledges hospitality from Southern University of Science and Technology and funding from the European Research Council (ERC) under the European Unions Horizon 2020 research and innovation programme (grant agreement No 882340).

Declaration of interests. The authors report no conflict of interest.

Appendix A.

According to the work (Parmar *et al.* 2012), the governing equation for the movement of light particles in compressible turbulence can be expressed as below (neglecting history force):

$$\rho_p \frac{d\mathbf{v}_p}{dt} = \frac{9\mu}{2a^2} (\mathbf{u}_p - \mathbf{v}_p) + \rho_f \frac{D\mathbf{u}_p}{Dt} + \frac{1}{2} \left[\frac{D(\rho_f \mathbf{u}_p)}{Dt} - \frac{d(\rho_f \mathbf{v}_p)}{dt} \right] \quad (\text{A } 1)$$

$$\frac{d\mathbf{v}_p}{dt} = \frac{\mathbf{u}_p - \mathbf{v}_p}{\tau_p} + \beta \frac{D\mathbf{u}_p}{Dt} + \frac{\beta}{3\rho_f} \left[\mathbf{u}_p \frac{D\rho_f}{Dt} - \mathbf{v}_p \frac{d\rho_f}{dt} \right] \quad (\text{A } 2)$$

from mass conservation equation, we have

$$\frac{D\rho_f}{Dt} = -\rho_f \nabla \cdot \mathbf{u} \quad (\text{A } 3)$$

$$\frac{d\rho_f}{dt} = \frac{D\rho_f}{Dt} + (\mathbf{v}_p - \mathbf{u}_p) \cdot \nabla \rho_f \quad (\text{A } 4)$$

substituting Eq. (A 3) and Eq. (A 4) into Eq. (A 2), we get

$$\frac{d\mathbf{v}_p}{dt} = \frac{\mathbf{u}_p - \mathbf{v}_p}{\tau_p} + \beta \frac{D\mathbf{u}_p}{Dt} + \left\{ \frac{\beta}{3} (\mathbf{v}_p - \mathbf{u}_p) \nabla \cdot \mathbf{u}_p - \frac{\beta}{3\rho_f} \mathbf{v}_p [(\mathbf{v}_p - \mathbf{u}_p) \cdot \nabla \rho_f] \right\} \quad (\text{A } 5)$$

If St is small (τ_p is quite small), $(\mathbf{v}_p - \mathbf{u}_p)$ in the third term at the right hand side (RHS) of Eq. (A 5) will be also small as $\mathbf{v}_p = \mathbf{u}_p + O(\tau_p)$. However, in compressible flows, $\nabla \cdot \mathbf{u}_p$ and $\nabla \rho_f$ will increase as M_t increases. Consequently, there is a question whether the contribution of the third term at RHS of Eq. (A 5) can be neglected. Here, we define

$$F_1 = \left| \frac{\mathbf{u}_p - \mathbf{v}_p}{\tau_p} \right|$$

$$F_2 = \left| \beta \frac{D\mathbf{u}_p}{Dt} \right|$$

$$F_3 = \left| \frac{\beta}{3} (\mathbf{v}_p - \mathbf{u}_p) \nabla \cdot \mathbf{u}_p - \frac{\beta}{3\rho_f} \mathbf{v}_p [(\mathbf{v}_p - \mathbf{u}_p) \cdot \nabla \rho_f] \right|$$

and then measure the averages of F_1 , F_2 and F_3 among all particles at different time slices, in order to have an a priori estimate of the importance of the neglected terms. In Fig. 17 we show that the contribution of F_3 is well below 5% up to $M_t = 0.6$ and becomes

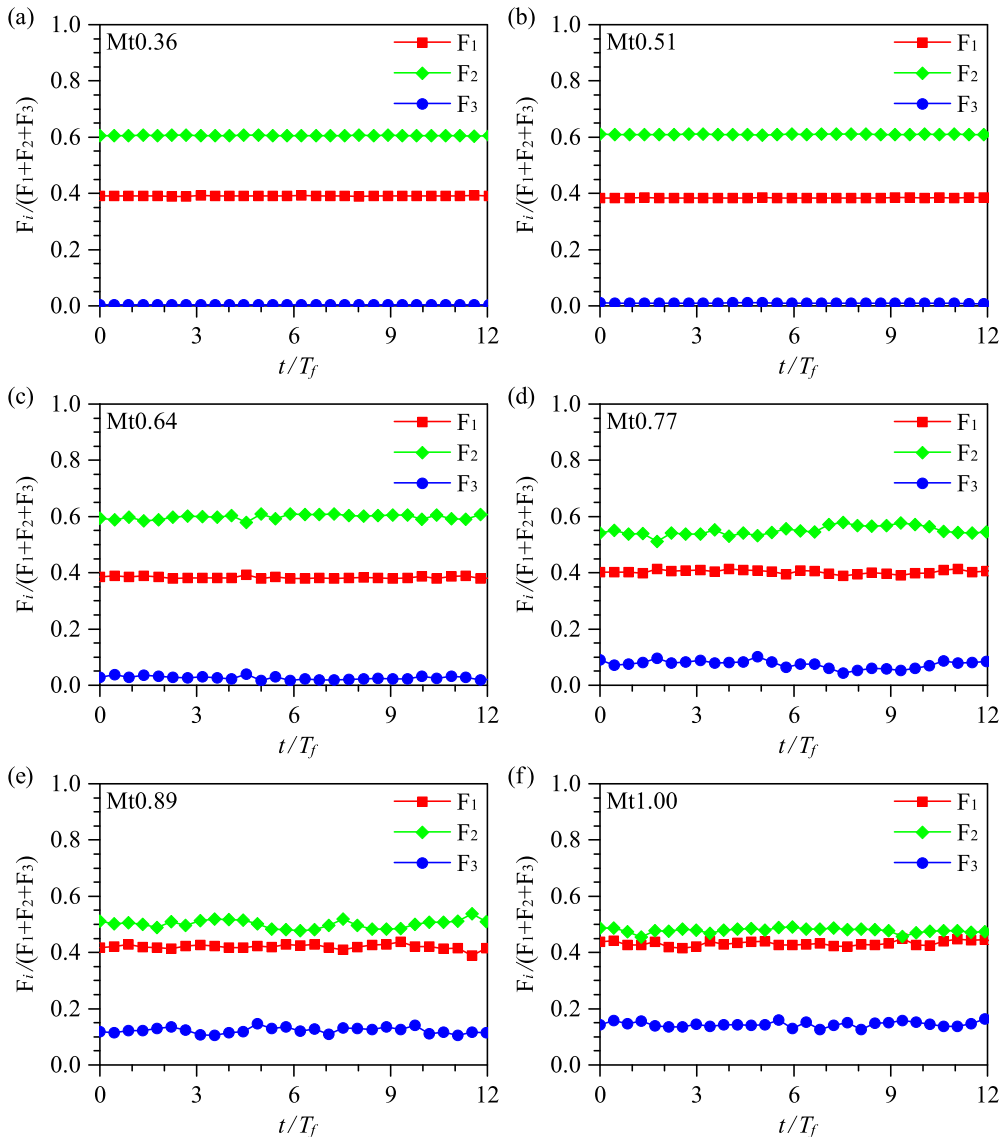


FIGURE 17. The average values of F_1 , F_2 and F_3 among all particles at different time slices

of the order of 10 – 15% only at the largest Mach number $M_t = 1.00$. As a result, we argue that the approximation we made is reasonably acceptable up to the largest Mach number we have investigated and we leave for future studies the question to check the precise impact of the extra terms in (A 5) for those Mach regimes.

REFERENCES

- ANDERSON JR, JOHN DAVID 2010 *Fundamentals of aerodynamics*. Tata McGraw-Hill Education.
- AYYALASOMAYAJULA, SATHYANARAYANA, GYLFASON, ARMANN, COLLINS, LANCE R, BODENSCHATZ, EBERHARD & WARHAFT, ZELLMAN 2006 Lagrangian measurements of inertial particle accelerations in grid generated wind tunnel turbulence. *Physical Review Letters* **97** (14), 144507.

- AYYALASOMAJULA, S, WARHAFT, Z & COLLINS, LR 2008 Modeling inertial particle acceleration statistics in isotropic turbulence. *Physics of Fluids* **20** (9), 095104.
- BARTH, ERIKA L & RAFKIN, SCOT CR 2007 Trams: A new dynamic cloud model for titan's methane clouds. *Geophysical Research Letters* **34** (3).
- BEC, J, BIFERALE, L, BOFFETTA, G, CELANI, A, CENCINI, M, LANOTTE, A, MUSACCHIO, S & TOSCHI, F 2006 Acceleration statistics of heavy particles in turbulence. *Journal of Fluid Mechanics* **550**, 349–358.
- BIFERALE, L, BOFFETTA, GUIDO, CELANI, ANTONIO, DEVENISH, BJ, LANOTTE, ALESSANDRA & TOSCHI, FEDERICO 2004 Multifractal statistics of lagrangian velocity and acceleration in turbulence. *Physical review letters* **93** (6), 064502.
- BIFERALE, LUCA & TOSCHI, FEDERICO 2005 Joint statistics of acceleration and vorticity in fully developed turbulence. *Journal of Turbulence* (6), N40.
- BOFFETTA, GUIDO & SOKOLOV, IGOR M 2002a Relative dispersion in fully developed turbulence: the richardson's law and intermittency corrections. *Physical review letters* **88** (9), 094501.
- BOFFETTA, GUIDO & SOKOLOV, IGOR M 2002b Statistics of two-particle dispersion in two-dimensional turbulence. *Physics of fluids* **14** (9), 3224–3232.
- BRAGG, ANDREW D, IRELAND, PETER J & COLLINS, LANCE R 2015a Mechanisms for the clustering of inertial particles in the inertial range of isotropic turbulence. *Physical Review E* **92** (2), 023029.
- BRAGG, ANDREW D, IRELAND, PETER J & COLLINS, LANCE R 2015b On the relationship between the non-local clustering mechanism and preferential concentration. *Journal of Fluid Mechanics* **780**, 327–343.
- CHUN, JAEHUN, KOCH, DONALD L, RANI, SARMA L, AHLUWALIA, ARUJ & COLLINS, LANCE R 2005 Clustering of aerosol particles in isotropic turbulence. *Journal of Fluid Mechanics* **536**, 219–251.
- COLEMAN, SW & VASSILICOS, JC 2009 A unified sweep-stick mechanism to explain particle clustering in two-and three-dimensional homogeneous, isotropic turbulence. *Physics of Fluids* **21** (11), 113301.
- CURRAN, ET, HEISER, WH & PRATT, DT 1996 Fluid phenomena in scramjet combustion systems. *Annual Review of Fluid Mechanics* **28** (1), 323–360.
- DAI, QI, JIN, TAI, LUO, KUN & FAN, JIANREN 2018 Direct numerical simulation of particle dispersion in a three-dimensional spatially developing compressible mixing layer. *Physics of Fluids* **30** (11), 113301.
- DAI, QI, LUO, KUN, JIN, TAI & FAN, JIANREN 2017 Direct numerical simulation of turbulence modulation by particles in compressible isotropic turbulence. *Journal of Fluid Mechanics* **832**, 438–482.
- FALKOVICH, G., FOUXON, A. & STEPANOV, M. G. 2002 Acceleration of rain initiation by cloud turbulence. *Nature* **419** (6903), 151–154.
- FEDERRATH, CHRISTOPH, ROMAN-DUVAL, J, KLESSEN, RS, SCHMIDT, WOLFGANG & MAC LOW, M-M 2010 Comparing the statistics of interstellar turbulence in simulations and observations-solenoidal versus compressive turbulence forcing. *Astronomy & Astrophysics* **512**, A81.
- FERRI, ANTONIO 1973 Mixing-controlled supersonic combustion. *Annual Review of Fluid Mechanics* **5** (1), 301–338.
- FUSTER, DANIEL & COLONIUS, TIM 2011 Modelling bubble clusters in compressible liquids. *Journal of Fluid Mechanics* **688**, 352–389.
- GATIGNOL, RENÉE 1983 The faxén formulae for a rigid particle in an unsteady non-uniform stokes flow. *Journal De Mécanique théorique et appliquée* **1** (2), 143–160.
- GOTO, SUSUMU & VASSILICOS, JC 2008 Sweep-stick mechanism of heavy particle clustering in fluid turbulence. *Physical review letters* **100** (5), 054503.
- GOTOH, TOSHIYUKI & ROGALLO, ROBERT S 1999 Intermittency and scaling of pressure at small scales in forced isotropic turbulence. *Journal of Fluid Mechanics* **396**, 257–285.
- HAUGEN, NEL, BRANDENBURG, A, SANDIN, C & MATTSSON, L 2021 Spectral characterisation of inertial particle clustering in turbulence. *arXiv e-prints* pp. arXiv–2105.
- HEISENBERG, WERNER 1985 Zur statistischen theorie der turbulenz. In *Original Scientific Papers Wissenschaftliche Originalarbeiten*, pp. 82–111. Springer.

- HUETE, CÉSAR, URZAY, JAVIER, SÁNCHEZ, ANTONIO L & WILLIAMS, FORMAN A 2016 Weak-shock interactions with transonic laminar mixing layers of fuels for high-speed propulsion. *AIAA Journal* **54** (3), 966–979.
- JOHANSEN, ANDERS, OISHI, JEFFREY S, MAC LOW, MORDECAI-MARK, KLAHR, HUBERT, HENNING, THOMAS & YODIN, ANDREW 2007 Rapid planetesimal formation in turbulent circumstellar disks. *Nature* **448** (7157), 1022–1025.
- JULLIEN, MARIE-CAROLINE, PARET, JÉRÔME & TABELING, PATRICK 1999 Richardson pair dispersion in two-dimensional turbulence. *Physical review letters* **82** (14), 2872.
- KIDA, SHIGEO & ORSZAG, STEVEN A 1990 Energy and spectral dynamics in forced compressible turbulence. *Journal of Scientific Computing* **5** (2), 85–125.
- KOLMOGOROV, ANDREY NIKOLAEVICH 1941a Dissipation of energy in the locally isotropic turbulence. *Dokl. Akad. Nauk SSSR* **31**, 538–540.
- KOLMOGOROV, ANDREY NIKOLAEVICH 1941b The local structure of turbulence in incompressible viscous fluid for very large reynolds numbers. *Dokl. Akad. Nauk SSSR* **30**, 301–305.
- LA PORTA, ARTHUR, VOTH, GREG A, CRAWFORD, ALICE M, ALEXANDER, JIM & BODENSCHATZ, EBERHARD 2001 Fluid particle accelerations in fully developed turbulence. *Nature* **409** (6823), 1017–1019.
- LAVEZZO, V, SOLDATI, A, GERASHCHENKO, S, WARHAFT, Z & COLLINS, LR 2010 On the role of gravity and shear on inertial particle accelerations in near-wall turbulence. *Journal of fluid mechanics* **658**, 229.
- MAXEY, MR 1987 The gravitational settling of aerosol particles in homogeneous turbulence and random flow fields. *Journal of Fluid Mechanics* **174**, 441–465.
- MAXEY, MARTIN R & RILEY, JAMES J 1983 Equation of motion for a small rigid sphere in a nonuniform flow. *The Physics of Fluids* **26** (4), 883–889.
- MORDANT, NICOLAS, CRAWFORD, ALICE M & BODENSCHATZ, EBERHARD 2004 Three-dimensional structure of the lagrangian acceleration in turbulent flows. *Physical review letters* **93** (21), 214501.
- NI, RUI, HUANG, SHI-DI & XIA, KE-QING 2012 Lagrangian acceleration measurements in convective thermal turbulence. *Journal of fluid mechanics* **692**, 395.
- ONISHI, RYO & VASSILICOS, JC 2014 Collision statistics of inertial particles in two-dimensional homogeneous isotropic turbulence with an inverse cascade. *Journal of Fluid Mechanics* **745**, 279–299.
- OTT, SØREN & MANN, JAKOB 2000 An experimental investigation of the relative diffusion of particle pairs in three-dimensional turbulent flow. *Journal of Fluid Mechanics* **422**, 207–223.
- PAN, LIUBIN, PADOAN, PAOLO, SCALO, JOHN, KRITSUK, ALEXEI G & NORMAN, MICHAEL L 2011 Turbulent clustering of protoplanetary dust and planetesimal formation. *The Astrophysical Journal* **740** (1), 6.
- PARMAR, MANOJ, HASELBACHER, ALLEN & BALACHANDAR, SIVARAMAKRISHNAN 2011 Generalized basset-boussinesq-oseen equation for unsteady forces on a sphere in a compressible flow. *Physical review letters* **106** (8), 084501.
- PARMAR, M, HASELBACHER, A & BALACHANDAR, S 2012 Equation of motion for a sphere in non-uniform compressible flows. *Journal of fluid mechanics* **699**, 352.
- REISMAN, GE, WANG, Y-C & BRENNEN, CHRISTOPHER E 1998 Observations of shock waves in cloud cavitation. *Journal of Fluid Mechanics* **355**, 255–283.
- SOMMERFELD, MARTIN 2001 Validation of a stochastic lagrangian modelling approach for inter-particle collisions in homogeneous isotropic turbulence. *International Journal of Multiphase Flow* **27** (10), 1829–1858.
- STELZENMULLER, NICKOLAS, POLANCO, JUAN IGNACIO, VIGNAL, LAURE, VINKOVIC, IVANA & MORDANT, NICOLAS 2017 Lagrangian acceleration statistics in a turbulent channel flow. *Physical Review Fluids* **2** (5), 054602.
- URZAY, JAVIER 2018 Supersonic combustion in air-breathing propulsion systems for hypersonic flight. *Annual Review of Fluid Mechanics* **50**, 593–627.
- VANCE, MARION W, SQUIRES, KYLE D & SIMONIN, OLIVIER 2006 Properties of the particle velocity field in gas-solid turbulent channel flow. *Physics of Fluids* **18** (6), 063302.
- VEDULA, PRAKASH & YEUNG, PUI-KUEN 1999 Similarity scaling of acceleration and pressure

- statistics in numerical simulations of isotropic turbulence. *Physics of Fluids* **11** (5), 1208–1220.
- VOLK, R, CALZAVARINI, ENRICO, VERHILLE, G, LOHSE, DETLEF, MORDANT, N, PINTON, J-F & TOSCHI, FEDERICO 2008*a* Acceleration of heavy and light particles in turbulence: comparison between experiments and direct numerical simulations. *Physica D: Nonlinear Phenomena* **237** (14-17), 2084–2089.
- VOLK, R, MORDANT, N, VERHILLE, G & PINTON, J-F 2008*b* Laser doppler measurement of inertial particle and bubble accelerations in turbulence. *EPL (Europhysics Letters)* **81** (3), 34002.
- VOTH, GA, LA PORTA, A, CRAWFORD, AM, ALEXANDER, J & BODENSCHATZ, E 2002 Measurement of particle accelerations in fully developed turbulence. *Journal of Fluid Mechanics* **469**, 121–160.
- VOTH, GREG A, SATYANARAYAN, K & BODENSCHATZ, EBERHARD 1998 Lagrangian acceleration measurements at large reynolds numbers. *Physics of Fluids* **10** (9), 2268–2280.
- WANG, JIANCHUN, WANG, L-P, XIAO, ZUOLI, SHI, Y & CHEN, S 2010 A hybrid numerical simulation of isotropic compressible turbulence. *Journal of Computational Physics* **229** (13), 5257–5279.
- WANG, LIAN-PING, WEXLER, ANTHONY S & ZHOU, YONG 1998 On the collision rate of small particles in isotropic turbulence. i. zero-inertia case. *Physics of fluids* **10** (1), 266–276.
- WANG, YI CHUN & BRENNEN, CHRISTOPHER E 1999 Numerical computation of shock waves in a spherical cloud of cavitation bubbles. *Journal of Fluids Engineering, Transactions of the ASME* **121** (4), 872–880.
- WILKINSON, MICHAEL, MEHLIG, BERNHARD & BEZUGLYY, VLAD 2006 Caustic activation of rain showers. *Physical Review Letters* **97**, 048501.
- XIAO, WEI, JIN, TAI, LUO, KUN, DAI, QI & FAN, JIANREN 2020 Eulerian–lagrangian direct numerical simulation of preferential accumulation of inertial particles in a compressible turbulent boundary layer. *Journal of Fluid Mechanics* **903**.
- XU, HAITAO, OUELLETTE, NICHOLAS T & BODENSCHATZ, EBERHARD 2007*a* Curvature of lagrangian trajectories in turbulence. *Physical review letters* **98** (5), 050201.
- XU, HAITAO, OUELLETTE, NICHOLAS T, VINCENZI, DARIO & BODENSCHATZ, EBERHARD 2007*b* Acceleration correlations and pressure structure functions in high-reynolds number turbulence. *Physical review letters* **99** (20), 204501.
- YAGLOM, AM 1949 On the acceleration field in a turbulent flow. *CR Akad. USSR* **67**, 795–798.
- YAMAMOTO, YASUFUMI, POTTHOFF, MATTHIAS, TANAKA, TOSHITSUGU, KAJISHIMA, TSUI & TSUJI, YUTAKA 2001 Large-eddy simulation of turbulent gas-particle flow in a vertical channel: effect of considering inter-particle collisions. *Journal of Fluid Mechanics* **442**, 303.
- YANG, YANTAO, WANG, JIANCHUN, SHI, YIPENG, XIAO, ZUOLI, HE, XT & CHEN, SHIYI 2013 Acceleration of passive tracers in compressible turbulent flow. *Physical review letters* **110** (6), 064503.
- YANG, YANTAO, WANG, JIANCHUN, SHI, YIPENG, XIAO, ZUOLI, HE, XT & CHEN, SHIYI 2014 Interactions between inertial particles and shocklets in compressible turbulent flow. *Physics of fluids* **26** (9), 091702.
- YANG, YANTAO, WANG, JIANCHUN, SHI, YIPENG, XIAO, ZUOLI, HE, XT & CHEN, SHIYI 2016 Intermittency caused by compressibility: a lagrangian study. *Journal of Fluid Mechanics* **786**.
- YEUNG, PK 1997 One-and two-particle lagrangian acceleration correlations in numerically simulated homogeneous turbulence. *Physics of Fluids* **9** (10), 2981–2990.
- YEUNG, PUI-KUEN & POPE, STEPHEN B 1989 Lagrangian statistics from direct numerical simulations of isotropic turbulence. *Journal of Fluid Mechanics* **207**, 531–586.
- ZHANG, QINGQING, LIU, HAN, MA, ZONGQIANG & XIAO, ZUOLI 2016 Preferential concentration of heavy particles in compressible isotropic turbulence. *Physics of Fluids* **28** (5), 055104.
- ZHANG, QINGQING & XIAO, ZUOLI 2018 Single-particle dispersion in compressible turbulence. *Physics of Fluids* **30** (4), 040904.
- ZHANG, ZHENTONG, LEGENDRE, DOMINIQUE & ZAMANSKY, RÉMI 2019 Model for the dynamics of micro-bubbles in high-reynolds-number flows. *Journal of Fluid Mechanics* **879**, 554–578.

ZHOU, YONG, WEXLER, ANTHONY S & WANG, LIAN-PING 1998 On the collision rate of small particles in isotropic turbulence. ii. finite inertia case. *Physics of fluids* **10** (5), 1206–1216.